Adsorption (2013) 19:305–321
DOI 10.1007/s10450-012-9453-8

Confined space effects driving to heterogenization of solutions at the interfaces

V.M. Gun'ko · V.V. Turov · R. Leboda · J. Skubiszewska-Zięba · B. Charmas

Received: 23 September 2012 / Accepted: 7 December 2012 / Published online: 22 December 2012

Abstract Water and concentrated solutions of acids (HCl, H_3PO_4, and H_3PO_3) or H_2O_2 are clustered at the interfaces of nanosilicas and multi-layer graphene oxide (MLGO) as shown by low-temperature ^{1}H NMR spectroscopy. The acid solutions in contact with silica or MLGO powders placed in nonpolar (CCl_4) or weakly polar ($CDCl_3$) media form nanodomains and clusters of several types and sizes with different contents of water and solutes. This differentiation of the solutions is stronger at a surface of more compacted nanosilicas because of enhanced confinement effects in narrower pores (voids) between adjacent nanoparticles. For MLGO, the confined space effects are relatively weak but the formation of ice crystallites during freezing of the suspension changes the material texture. Obtained results are of importance for deeper insight into the mechanism of the interfacial behavior of complex solutions under different confined space effects and due to the influence of organic co-solvents.

Keywords Nanosilica · Multilayer graphene oxide · Interfacial water · HCl solution · Phosporus oxyacids · H_2O_2 · Low temperature ^{1}H NMR spectroscopy · Cryoporometry

1 Introduction

The behavior of water as a unique compound possessing numerous unusual properties (Chaplin 2011) depends strongly on surroundings, confined space effects in pores with hydrophobic or hydrophilic surfaces, dissolved compounds content, temperature, etc. (Derjaguin et al. 1987, 1989; Israelachvili and Wennerstrom 1990; Mitchell et al. 2008; Petrov and Furó 2009). One of consequences of these effects is a diminution of water activity as a solvent located in pores that is enhanced with decreasing temperature and narrowing pores (Gun'ko et al. 2005, 2009; Mitchell et al. 2008; Petrov and Furó 2009; Chaplin 2011). These effects are of great significance due to their appearance in practical applications of hydrated or porous materials, solutions, mixtures, etc.

Results of previous studies of the interfacial behavior of water in mixtures with different organic co-solvents, ice-nucleators, polymers, and biomacromolecules interacting with activated carbons, graphene oxides, exfoliated graphite, nanosilicas, silica gels, porous polymers, etc. suggest that the mentioned effects can be studied using low-temperature ^{1}H NMR spectroscopy with a relatively narrow bandwidth and static samples, as well as by related NMR cryoporometry and relaxometry (Gun'ko et al. 2005, 2009; Turov and Gun'ko 2011). These studies showed the difference in the behavior of adsorbed binary or ternary mixtures of miscible solvents and water co-adsorbed with poorly miscible or immiscible organics. Confined space effects lead to enhanced clusterization (heterogenization) not only of the immiscible liquids but also of the solutions. The mechanisms of these effects are complex due to simultaneous action of different factors. Therefore, additional investigations of the effects of confined space, temperature and component concentrations for binary and ternary mixtures, solutions of acid (phosphorus oxyacids, HCl, H_2O_2) or co-adsorbed immiscible liquids should be carried out.

Typically, phosphorus oxyacids (POA) are used in aqueous solutions, in which POA molecules are strongly hy-

V.M. Gun'ko (✉) · V.V. Turov
Chuiko Institute of Surface Chemistry, 17 General Naumov Str., Kiev 03164, Ukraine
e-mail: vlad_gunko@ukr.net

R. Leboda · J. Skubiszewska-Zięba · B. Charmas
Faculty of Chemistry, Maria Curie-Skłodowska University, 20031 Lublin, Poland

drated but only partially deprotonated. Phosphorus oxyacids are well water-soluble but relatively weak acids with a low degree of dissociation of PO–H bonds in the aqueous solution (Nekrasov 1973). Chemical shift of the proton resonance (δ_H) in the ^{1}H NMR spectra of POA in concentrated aqueous solutions can reach 10 ppm or more (Emsley et al. 1965). This suggests the presence of hydrated protons appearing due to dissociation of a portion of the PO–H bonds. In phosphonic acid, doublet signals of protons from the P–H bonds are also observed due to large J-coupling to the P nuclei but of a lower intensity than that of the PO–H bonds (Schuster et al. 2008).

Dissociation and solvation of acids (e.g. HCl), which are relatively simple but important processes, can be used as model reactions. Mineral acids, such as hydrochloric acid, are strong acids, which are in completely dissociated state in diluted aqueous solutions (Drago 1977). This dissociation results in the formation of hydrated protons in clusters $H_3O^+(H_2O)_n$ (Eigen and Zundel cations) and acidic residua both strongly affecting the water structure (Jieli and Aida 2009). In the concentrated aqueous solutions, the dissociation degree of HCl is low (about several percents). This degree and the corresponding changes in water structure, depending on HCl concentration and the presence of silica nanoparticles, can be studied using ^{1}H NMR spectroscopy, comparing changes in the δ_H values for pure and maximum concentrated acids and pure water. 'Acidic' H atoms in the most numbers of acids are characterized by low electron density. Therefore the δ_H values can be of 9–13 ppm. However, this is smaller than δ_H = 16–20 ppm of protons in the strongest hydrogen bonds N···H–O according to experimental and theoretical results (Tolstoy et al. 2004; Murakhtina et al. 2006).

The physicochemical properties of hydrogen peroxide and water strongly differ (Jones 1999; Hess 1995; March 1992). This difference is caused first of all by the difference in their hydrogen bond network. Each H in H_2O_2 can interact with two O atoms from neighboring molecules. Each H in H_2O interacts with only one O atom in the hydrogen bonds. This results in clear difference in the ^{1}H NMR spectra of water and hydrogen peroxide, since the latter has higher δ_H values (Zhang 2007; Stephenson and Bell 2005). Low temperature ^{1}H NMR spectroscopy is a very informative method to study changes in the hydrogen network of water depending on the presence of H_2O_2 and organic cosolvents bound to adsorbent particles (Mitchell et al. 2008; Brennan et al. 2001).

This paper describes the investigations, which were carried out by low-temperature ^{1}H NMR spectroscopy, adsorption and quantum chemical methods, of concentrated solutions of strong acids such as HCl, phosphorus oxyacids (POA) H_3PO_4 and H_3PO_3, and H_2O_2 interacting with such adsorbents as nanosilicas and graphene oxide placed in different dispersion media. Despite the differences in the materials and adsorbates studied, there are certain regularities in the interfacial behavior of miscible and immiscible co-adsorbates such as water, acids and organic liquids of different polarity. The aim of this paper is to show the features of liquid co-adsorbates and aqueous solutions undergoing confined space effects in pores of different shapes and sizes in nanosilicas and multi-layer graphene oxide.

2 Experimental

Nanosilicas A-300 at bulk density $\rho_b = 0.045$ g/cm^3, A-400 at $\rho_b = 0.061$ g/cm^3 (Pilot plant of Chuiko Institute of Surface Chemistry, Kalush, Ukraine) and OX-50 (Degussa, $\rho_b = 0.13$ g/cm^3) were heated at 400 °C for several hours before the use. Additionally, initial A-300 was mechanochemically activated (MCA-A-300, ρ_b = 0.394 g/cm^3) in a ball mill for several hours with the presence of water (50 wt.% in respect to dry silica). Multilayer graphene oxide (MLGO) (CheapTubes Inc) was used in comparative investigations of water adsorbed alone or co-adsorbed with organic solvents and acids (Gun'ko et al. 2012b).

Distilled water, DCl (36 % solution in D_2O), solid and dissolved (in water) H_3PO_4 and H_3PO_3, 30 wt.% aqueous solution of H_2O_2 and solvents CD_3CN, C_6H_6, C_6D_6, $CHCl_3$, $CDCl_3$, $(CH_3)_2SO$, $(CD_3)_2SO$, and CCl_4 (grade for NMR spectroscopy) were used in ^{1}H NMR spectroscopy measurements of static samples (Turov et al. 2011; Gun'ko et al. 2012a, 2012b). The use of the DCl solution (including approximately 3 % of HCl), in which the D–H exchange occurs during contact with silica, provides a relatively low intensity of ^{1}H NMR signals appropriate for spectra recording. Concentrated aqueous suspension of OX-50 (16 wt.%) with 4 wt.% of H_3PO_4 was dried at 293 K for 8 days and then at 330 K for 10 min. According to calibrated NMR and thermogravimetric measurements, the residual content of water was 0.5 wt.%. To prepare more hydrated systems, certain amounts of water were added to the powder and equilibrated for 1 h. A-300/POA was prepared using A-300 powder mixed with a solution of H_3PO_4 in isopropanol, stirred and heated at 353–383 K for complete removal of the solvent. Initial solid H_3PO_3 included 50 mg of water per gram of acid. 30 wt.% POA solution was used in the study. The aqueous suspension of silica A-300/H_3PO_3 (ratio 4/1) was stirred and dried at 293 K for 14 days to obtain a powder with a low content of adsorbed water.

The ^{1}H NMR spectra were recorded at 200–320 K using a Varian 400 Mercury spectrometer (magnetic field of 9.4 T) of high resolution with the 90° probe pulses with duration of 2–3 μs. Relative mean errors were smaller than

±10 % for ^{1}H NMR signal intensity for overlapped signals and ±5 % for single signals, and ±1 K for temperature. To prevent supercooling of the systems, the temperature dependences of concentration of unfrozen water ($C_{uw}(T)$ determined from the total ^{1}H NMR signal using a calibration function, Gun'ko et al. 2005) alone or in solutions were determined during heating of samples pre-cooled to 200 K. Signals of water molecules from ice and adsorbents did not contribute the ^{1}H NMR spectra recorded here for static samples because of features of the measurement technique with a narrow bandwidth and short time of transverse relaxation of protons in solids (Gun'ko et al. 2005, 2009; Turov and Gun'ko 2011).

To prepare hydrated powders, certain amounts of distilled water and/or solutes or dissolved compounds were added to air-dry powder samples placed into NMR ampoules. Before the measurements, samples (placed in closed NMR ampoules) were shaken for 10 min and then equilibrated for 1 h (the samples were uniform in the sensor gap because the spectra were practical identical with sample rotation and without rotation). To determine the chemical shift of the proton resonance, δ_H, tetramethylsilane (TMS) was used as an internal standard (assuming $\delta_H = 0$ ppm over the total temperature range) added to organic solvents in amount of 0.2 wt.%. The ^{1}H NMR spectra recorded at different temperatures were used to determine the temperature dependences of the amounts of unfrozen water and changes in the Gibbs free energy ($\Delta G(T)$) of the mobile phase due to interaction with a surface of adsorbents (Gun'ko et al. 2005). The low-temperature ^{1}H NMR spectroscopy allows obtaining both structural information on interfacial water, pore structure (with cryoporometry) and the thermodynamic characteristics of bound water or other liquids. These characteristics include changes in the Gibbs free energy upon adsorption (ΔG) for strongly bound water (SBW), $\Delta G_s < -0.8$ kJ/mol, and weakly bound water (WBW), $\Delta G_w > -0.8$ kJ/mol, free surface energy (γ_S) calculated as the modulus of the integral of the $\Delta G(C_{uw}(T))$ function, and the amounts of SBW ($C_{uw}{}^s$) and WBW ($C_{uw}{}^w$). WBW is frozen at $T > 250$ K but SBW is frozen at $T < 250$ K (Gun'ko et al. 2005). Changes in the Gibbs free energy (ΔG) of ice with temperature (Glushko 1978) were calculated as follows:

$$\Delta G_{ice} = 0.0295 - 0.0413\Delta T + 6.64369 \times 10^{-5}(\Delta T)^2 + 2.27708 \times 10^{-8}(\Delta T)^3 \quad \text{(kJ/mol)}, \tag{1}$$

where $\Delta T = 273.16 - T$ at $T \le 273.15$ K. Equation (1) was used to estimate the $\Delta G(T)$ function for bound water. The fact that bound water may remain unfrozen at $T < 273$ K suggests that its Gibbs free energy remains lower than that of bulk water or bulk ice $G_w^i < G_{ice}$ because of interactions with a solid surface or co-adsorbates. Further lowering of temperature reduces this inequality until the point T_{pf}, at which a certain amount of bound water becomes frozen. At T_{pf} the relationship $\Delta G_w = \Delta G_{ice}$ pertains, where $\Delta G_w^i = G_w^i(T) - G_w^0$ (G_w^0 denotes the Gibbs free energy of unperturbed bulk water at 273.15 K and superscript i stands for interfaces). It is assumed that neither G_{ice}, nor ΔG_{ice} are influenced by the solid surface. The area under the $\Delta G(C_{uw})$ curve (temperature dependences $\Delta G(T)$ and amounts of unfrozen pore water $C_{uw}(T)$ can be simply transformed into the relationship $\Delta G(C_{uw})$) determines overall changes in the Gibbs free energy of interfacial water

$$\gamma_S = A \int_0^{C_{uw}^{max}} \Delta G dC_{uw}, \tag{2}$$

where C_{uw}^{max} is the total amount of unfrozen water at $T = 273$ K, and A is a constant dependent on the type of units used in this equation (Gun'ko et al. 2005).

Water can be frozen in narrower pores at lower temperatures as described by the Gibbs-Thomson relation for the freezing point depression for liquids confined in cylindrical pores at radius R (Strange et al. 1993; Gun'ko et al. 2005; Mitchell et al. 2008; Petrov and Furó 2009)

$$\Delta T_m = T_{m,\infty} - T_m(R) = -\frac{2\sigma_{sl} T_{m,\infty}}{\Delta H_f \rho R} = \frac{k}{R}, \tag{3}$$

where $T_m(R)$ is the melting temperature of ice in cylindrical pores of radius R, $T_{m,\infty}$ the bulk melting temperature, ΔH_f the bulk enthalpy of fusion, ρ the density of the solid, σ_{sl} the surface energy of the solid-liquid interface, and k is a constant dependent on the types of both adsorbate and adsorbent. Equation (3) and the $C_{uw}(T)$ functions were used to determine the distribution functions ($f_V(R) = dV_{uw}(R)/dR$, where $V_{uw}(R)$ is the volume of unfrozen water located in pores at radius R) of sizes of water structures unfrozen at $T < 273$ K adsorbed onto nanosilicas or MLGO. Notice that application of the NMR cryoporometry to a variety of solid and soft materials gave reliable structural characteristics compared with those based on the data of the standard adsorption methods (Mitchell et al. 2008; Petrov and Furó 2009; Gun'ko et al. 2005, 2009).

The textural characteristics of adsorbents were determined from low-temperature (77.4 K) nitrogen adsorption–desorption isotherms recorded using a Micromeritics ASAP 2405N adsorption analyzer. The specific surface area (S_{BET}) was calculated according to the standard BET method (Gregg and Sing 1982). The total pore volume V_p was evaluated from the nitrogen adsorption at $p/p_0 = 0.98$–0.99 (p and p_0 denote the equilibrium and saturation pressure of nitrogen at 77.4 K, respectively). The nitrogen desorption data were used to compute the pore size distributions (PSDs, differential $f_V(R) \sim dV_p/dR$ and $f_S(R) \sim dS/dR$) using a self-consistent regularization (SCR) procedure under non-negativity condition ($f_V(R) \ge 0$ at any pore radius R) at a fixed regularization parameter $\alpha = 0.01$ with

a complex pore model with slit-shaped and cylindrical pores and voids between spherical nonporous nanoparticles packed in random aggregates (SCV model) (Gun'ko et al. 2009). The differential PSDs (with respect to pore volume $f_V(R) \sim dV/dR$, $\int f_V(R)dR \sim V_p$) were re-calculated as incremental PSD (IPSD, $\sum \Phi_{V,i}(R) = V_p$). The differential $f_S(R)$ functions were used to estimate the deviation (Δw) of the pore shape from the model (Gun'ko and Mikhalovsky 2004). The $f_V(R)$ and $f_S(R)$ functions were also used to calculate contributions of nanopores (V_{nano} and S_{nano} at $0.35 < R < 1$ nm), mesopores (V_{meso} and S_{meso} at $1 < R < 25$ nm), and macropores (V_{macro} and S_{macro} at $25 < R < 100$ nm) to the total pore volume and surface area.

Quantum chemical calculations of water clusters with solutes were carried out with consideration of the solvation effects in different dispersion media (IEFPCM method (Frisch et al. 2004)) using the Gaussian 03 program package with the DFT (B3LYP/6-31G(d,p)) technique (Frisch et al. 2004). The NMR spectra were calculated using the gauge-independent atomic orbital (GIAO) method (Frisch et al. 2004) or correlation functions applied to atomic charges q_H in large systems calculated by semiempirical PM6 or PM7 methods (Stewart 2012).

3 Results and discussion

Primary nonporous nanoparticles of A-300 form relatively rigid aggregates and soft agglomerates of aggregates (Fig. 1) responsible for the textural porosity of the powder. The bulk density of nanosilicas powder is low ($\rho_b = 0.04$–0.13 g/cm^3 for the initial silicas) but it increases with average size of primary particles. Despite very large empty space in the powders ($V_{em} = 1/\rho_b - 1/\rho_0 = 7$–$25$ cm^3/g, where $\rho_0 \approx 2.2$ g/cm^3 is the true density of fumed silica), the pore volume determined from the nitrogen adsorption isotherms, V_p (Table 1) is much smaller than V_{em}. The textural porosity is responsible for the appearance of hysteresis loops in the nitrogen adsorption-desorption isotherms typical for mesoporous materials. Contributions of mesopores to the specific surface area (Table 1, S_{meso} and S_{BET}) and pore volume (V_{meso} and V_p) are predominant for all nanosilicas studied. The pore (void) size distributions are relative complex (Fig. 2) because of a complex structural hierarchy of primary and secondary particles in silicas (Fig. 1). MCA-A-300 is characterized by the PSD shifted towards narrower pore sizes in comparison with the initial A-300 because of

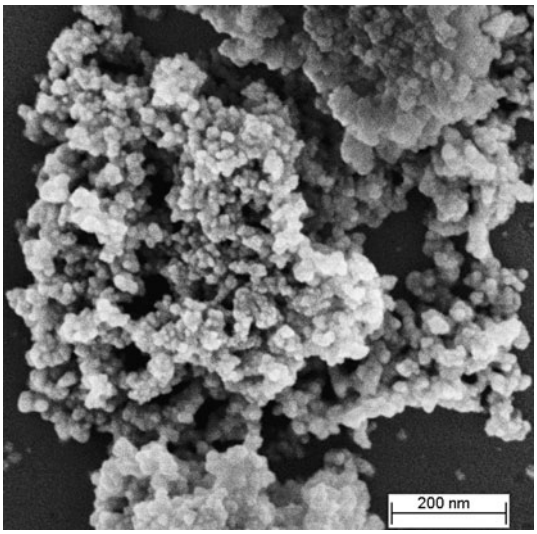

Fig. 1 SEM image of nanosilica A-300

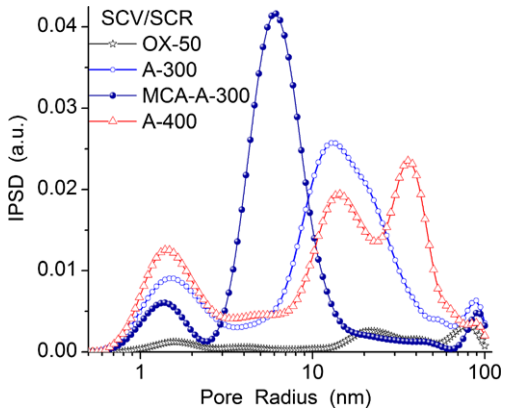

Fig. 2 Incremental pore size distributions for nanosilicas calculated with the SCV model using self-consistent regularization procedure (corresponding characteristics are shown in Table 1)

Table 1 Textural characteristics of nanosilicas (model SCV/SCR)

Sample	S_{BET} (m^2/g)	S_{nano} (m^2/g)	S_{meso} (m^2/g)	S_{macro} (m^2/g)	V_p (cm^3/g)	V_{nano} (cm^3/g)	V_{meso} (cm^3/g)	V_{macro} (cm^3/g)	Δw
A-400	409	64	327	18	0.859	0.033	0.550	0.276	0.388
A-300[a]	330	51	270	9	0.826	0.026	0.653	0.147	0.531
A-300[b]	332	29	301	2	0.771	0.017	0.714	0.040	0.376
OX-50	54	3	47	4	0.144	0.002	0.075	0.067	0.550

Note. [a]Initial silica and [b]MCA-A-300

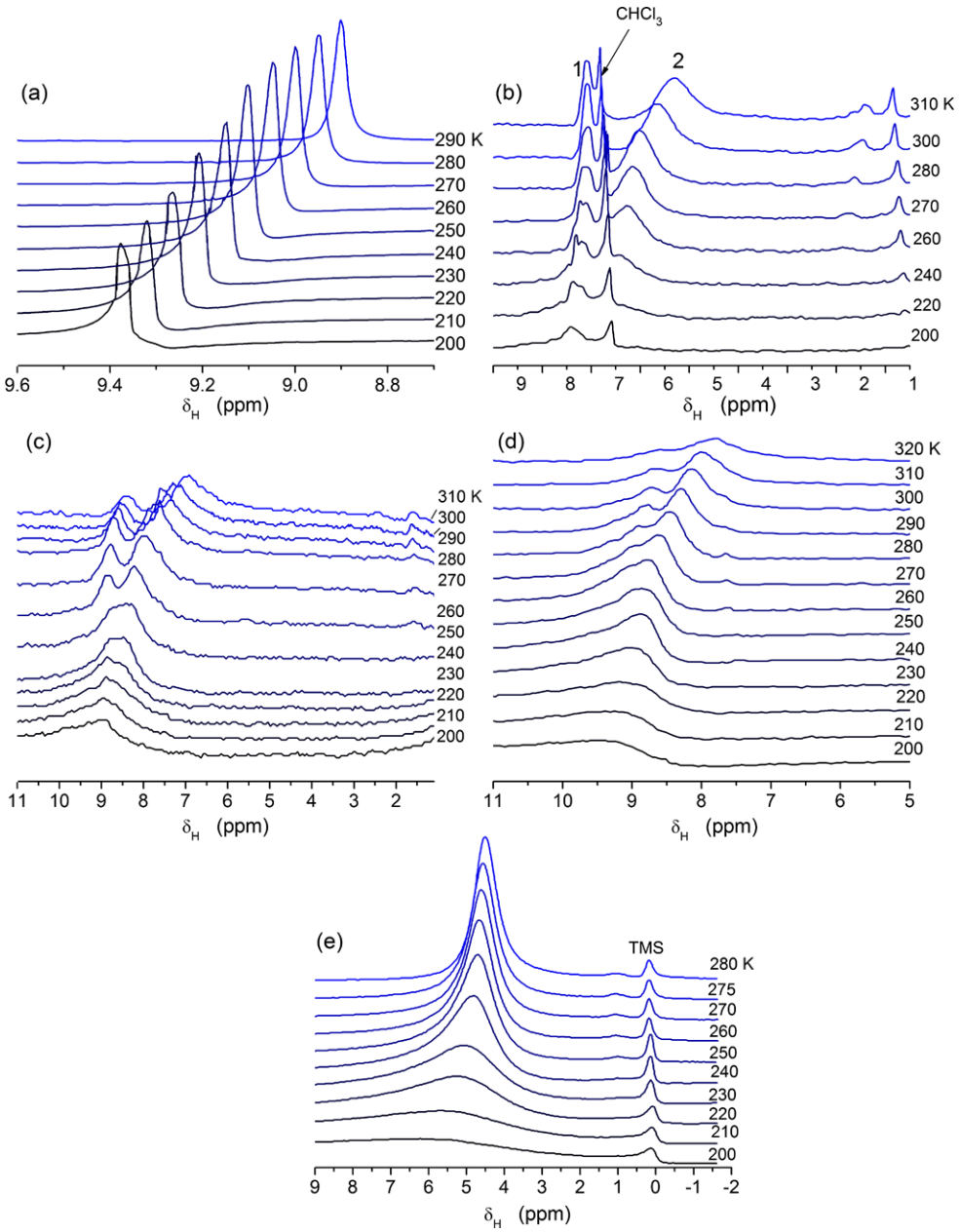

Fig. 3 ^{1}H NMR spectra at different temperatures of (**a**) 36 % hydrochloric acid, and hydrochloric acid and water adsorbed to (**b**)–(**d**) initial A-300 and (**e**) MCA-A-300 in (**b**) $CDCl_3$ or (**c**)–(**e**) CCl_4; (**b**), (**c**), (**e**) 38 mg/g H_2O and 44 mg/g HCl, (**d**) 140 mg/g H_2O and 120 mg/g HCl

significant compaction of agglomerates. OX-50 has minimal textural porosity since the larger the primary nanoparticles, the lower the aggregation of nanosilicas (Gun'ko et al. 2009). A-400 has a maximal contribution of narrow pores at $R < 3$ nm. The complex shape of secondary particles (Fig. 1) leads to relatively large Δw values (Table 1) showing the deviation of the pore shape from the SCV model. The difference in the textural characteristics of the initial A-300 and MCA-A-300, as well as A-400 and OX-50 (Fig. 2 and Table 1) can lead a different behavior of liquids such as water alone or co-adsorbed with miscible or immiscible liquids or acid solutions bound to the materials studied.

In 36 % hydrochloric acid used, in average six water molecules are per HCl molecule. This solution is unfrozen at $T > 200$ K (Fig. 3a) but water and HCl can be simultaneously frozen at $T < 200$ K (Leninsky et al. 1985). However, freezing of the HCl solution is possible at higher temperatures if the HCl concentration (C_{HCl}) decreases in the solution. Thus, the results shown in Figs. 3b–d can be interpreted as the formation of two types of HCl/water structures with different concentrations of HCl with different chemical shifts. The C_{HCl} value is smaller in structures corresponding to signal 2 at a lower δ_H value. These structures include mainly non-dissociated HCl molecules. The chemical shift of signal 1 is close to that of individual HCl solution

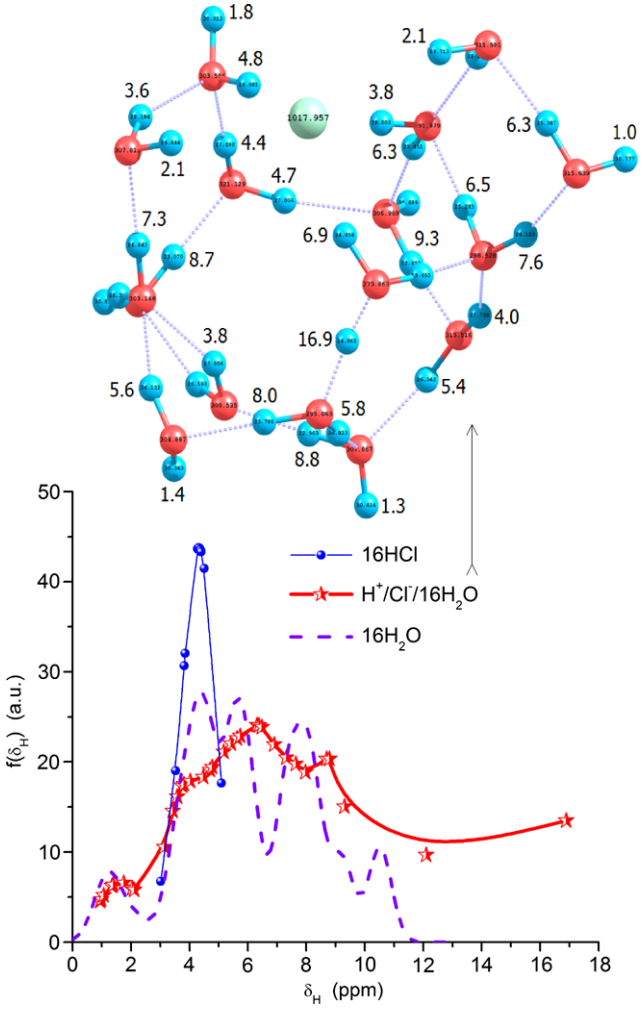

Fig. 4 The δ_H values in a cluster with dissociated HCl and $16H_2O$, and the distribution function of the δ_H values for clusters with 16HCl, $16H_2O$ and dissociated HCl interacting with $16H_2O$ (geometry was optimized using IEFPCM/B3LYP/6-31G(d,p) and the NMR spectra were calculated using GIAO with consideration of the solvation effects)

(Fig. 3a), i.e. the structures corresponding to signal 1 have the properties similar to that of the bulk HCl solution with significant contribution of dissociated HCl.

For water/HCl adsorbed onto MCA-A-300, the ^{1}H NMR spectra (Fig. 3e) are similar to that of water adsorbed on A-300 (Turov et al. 2011). Freezing of the adsorbates in these systems occurs at similar temperatures. Water in confined space of smaller voids in MCA-A-300 can have a lower activity as a solvent. Therefore, water (strongly associated water, SAW characterized by $\delta_H > 3.5$ ppm similar to bulk water at $\delta_H = 4.5$ ppm) adsorbed on MCA-A-300 dissolves a lower amount of HCl. Quantum chemical calculations of the ^{1}H NMR shielding tensors (chemical shifts, Fig. 4) converted into the spectra show that non-dissociated HCl molecules dissolved in water have $\delta_H < 6$ ppm that corresponds to signal observed in Fig. 3e.

An anhydrous cluster with 16HCl but calculated with consideration of the solvation effects (GIAO/IEFPCM/B3LYP/6-31G(d,p)) has a narrow $f(\delta_H)$ distribution function (Fig. 4) because all the HCl molecules are non-dissociated. In the case of a dissociated HCl molecule surrounded by $16H_2O$, a separated ion pair forms with H^+, in $H_5O_2^+$, and Cl^- interacting with several H_2O molecules (Fig. 4). The ^{1}H NMR spectra of the anhydrous cluster with 16HCl and of the water cluster with dissociated HCl strongly differ (Fig. 4). The latter has much broader ^{1}H NMR spectrum than non-dissociated 16HCl molecules and it is characterized by greater δ_H values up to 17 ppm. These calculations show that the position of the resonance peak (signal 2, Fig. 3b) can be affected by the presence of non-dissociated HCl. Eigen and Zundel cations located far from Cl^- ions (Murakhtina et al. 2006) provide signals at higher δ_H values (signal 1, Fig. 3b).

The properties of phosporus oxyacids, their interactions with water and interfacial behavior differ from those of HCl, however certain common features are characteristic for them due to the confined space effects (Turov and Gun'ko 2011; Gun'ko et al. 2012a). The ^{1}H NMR spectra of solid phosphonic acid with a low content of adsorbed water (50 mg per gram of solid POA) in CCl_4 medium include three signals at $\delta_H = 6$ ppm (signal 1), 5 ppm (weak signal 3 as a shoulder of signal 1) and 3.5 ppm (signal 2) at 290 K (Fig. 5a). The shape of signal 1 is asymmetrical. Its intensity decreases with decreasing temperature (Fig. 5a), as well as the δ_H value decreases to 5 ppm at $T = 200$ K in contrast to the behavior of signal in the concentrated POA solution (Gun'ko et al. 2012a). The δ_H values of signals 2 and 3 depend weaker on temperature than that of signal 1. An increase in the hydration degree to $h = 70$ mg/g results in an increase in the signal intensity and width (Fig. 5b). However, the temperature behavior of the spectra is similar to that at $h = 50$ mg/g.

The down-field shift of signal 1 with increasing temperature suggests that a relative contribution of Eigen and Zundel cations $H_3O^+(H_2O)_n$ in water with dissolved acid can increase with temperature (Fig. 5) because of increased solubility and deprotonation of H_3PO_3 with elevating temperature due to thawing of SAW frozen at low temperatures. However, contribution of hydrated protons (i.e. dissociated POA) is small at low content of water (Fig. 5a). Therefore, the δ_H value decreases with decreasing temperature (Fig. 5) in contrast to that for the concentrated POA solution (Gun'ko et al. 2012a). The spectra shape shows that structures with water/dissolved H_3PO_3 are nonuniform, since several signals are observed. Signal 2 at 3.5 ppm can be attributed to water molecules with one hydrogen bond per H_2O as a proton-donor and to PO–H without the hydrogen bonding. Signal 3 corresponds to SAW practically without dissolved acid in contrast to water/acid solution with signal 1.

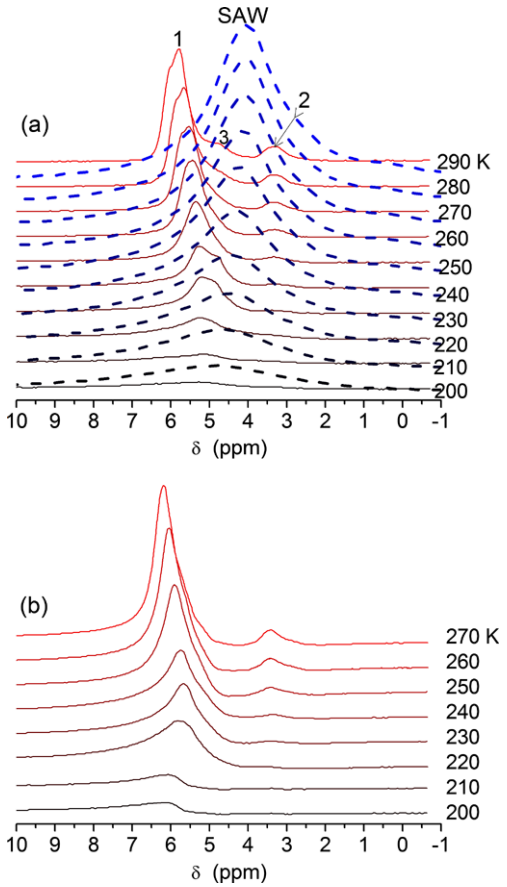

Fig. 5 ^{1}H NMR spectra recorded at different temperatures of weakly hydrated solid phosphonic acid (**a**), (**b**) alone and ((**a**), *dashed lines*) adsorbed onto nanosilica at A-300/POA = 4/1 at h = (**a**) 50, (**b**) 70 and ((**a**), *dashed lines*) 100 mg/g in CCl_4 medium

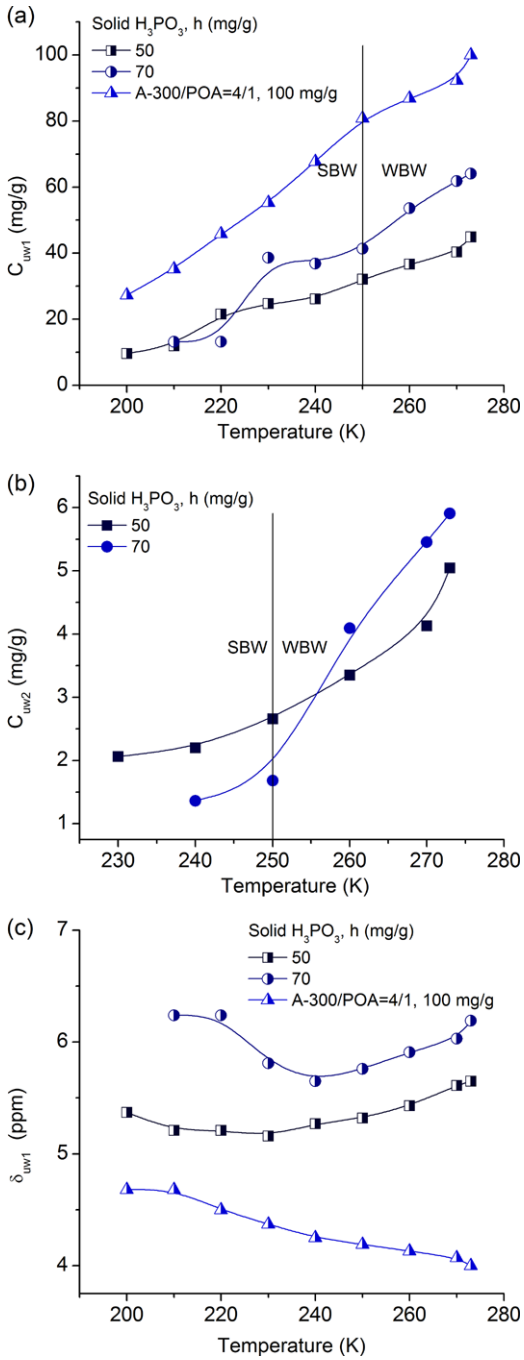

Fig. 6 Temperature dependences of concentration of unfrozen water responsible for signal (**a**) 1 and (**b**) 2 and (**c**) chemical shift of signal 1 for weakly hydrated solid H_3PO_3 (C_{H_2O} = 50 or 70 mg/g) and A-300/H_3PO_3 = 4/1 (C_{H_2O} = 100 mg/g) in CCl_4 medium

Dried suspension with 16 wt.% of silica and 4 wt.% of H_3PO_3 as a powder with approximately 10 wt.% of water (determined using a calibration function, Gun'ko et al. 2005) is characterized by the ^{1}H NMR spectra with only one relatively broad signal at 4.0-4.5 ppm (Fig. 5a, dashed lines), i.e. SAW with a very small amount of dissolved acid. Similarly to hydrated nanosilica, A-300 modified by phosphonic acid obtained by hydrolysis of adsorbed PCl_3 was characterized by a larger shift at δ_H = 6.5–10.5 ppm (Turov et al. 1996). During drying of the concentrated suspension with silica and POA, solution supersaturation results in the formation of acid crystallites. Additionally, water (at a low content) bound to nanosilica has low activity as a solvent. According to the ^{1}H NMR spectra (Fig. 5a), bound water can dissolve a small amount of H_3PO_3. Therefore, the δ_H value depends weakly on temperature as well as the signal shape.

Water unfrozen at $T < 273$ K due to bonding to solid POA or dried A-300/POA powder (Fig. 6a) includes both strongly bound water (SBW unfrozen at $T < 250$ K at $-\Delta G > 0.8$ kJ/mol) and weakly bound water (WBW frozen at $T < 250$ K at $-\Delta G < 0.8$ kJ/mol) (Gun'ko et al. 2005, 2009). However, there is no a clear boundary between SBW and WBW structures because of changes in the concentration of dissolved POA with temperature. A major fraction of water responsible for signal 1 ($C_{uw1}(T)$) (Fig. 6a) corresponds to SBW but a major fraction of water giving signal 2 corresponds to WBW (Fig. 6b).

Table 2 Characteristics of water bound in POA or POA/silica powders

Sample	h (mg/g)	S_{uw} (m^2/g)	S_{nano} (m^2/g)	S_{dom} (m^2/g)	V_{nano} (cm^3/g)	V_{dom} (cm^3/g)	γ_S (J/g)
H_3PO_3 (signal 1)	50	30	26	4	0.011	0.030	4.1
H_3PO_3 (signal 2)	50	0.4	0	0.4	0	0.004	0.6
H_3PO_3 (signal 1)	70	32	24	8	0.010	0.051	5.3
H_3PO_3 (signal 2)	70	0.6	0	0.6	0	0.006	0.3
H_3PO_3/A-300	100	82	74	8	0.032	0.062	9.8
H_3PO_4/OX-50	5	1	0	1	0	0.005	0.5
H_3PO_4/OX-50	25	12	10	2	0.005	0.010	1.7
H_3PO_4/OX-50	45	16	12	4	0.006	0.034	3.3
H_3PO_4/OX-50*	4000	651	374	277	0.169	1.624	110

Note. *Concentrated aqueous suspension but other samples are weakly hydrated powders

The δ_H value for a sample with 50 mg of water per gram of acid depends weakly on temperature (Fig. 6c). It slightly increases at $T > 230$ K. An increase in the water content to 70 mg/g gives an increase in the δ_H value with a minimum at 240 K. For the dried A-300/H_3PO_3 powder, the δ_H value decreases with increasing temperature (Fig. 6c). These results are caused by such two competitive processes as a diminution of associativity of water molecules (δ_H decreases) and an increase in concentration of dissolved acid with temperature (δ_H increases).

During freezing of the solution, pure ice and acid crystallites (which do not contribute the ^{1}H NMR spectra here) form separately. However, interfacial water can be frozen at lower temperature than acid that affect the concentration of acid dissolved in the interfacial water and the chemical shift δ_H decreases with lowering temperature. However, signal of the concentrated acid solution is absent in weakly hydrated A-300/H_3PO_3 powder. This is due to a low activity of water bound to the silica surface. This water does not dissolve the acid which forms crystallites weakly bound to the silica surface.

Solid POA has a relatively low surface area, which is in contact with unfrozen water at low h values (Table 2, S_{uw}), and clusters of water at $R < 1$ nm give a major contribution to the S_{uw} value (Table 2, S_{nano}). However, the volume of water clusters (Table 2, V_{nano}) is smaller than the volume of larger domains (V_{dom}) of unfrozen water at $1 < R < 25$ nm. Addition of water (to 70 mg/g) enhances mainly contribution of domain structures (S_{dom}, V_{dom}). Signal 2 (Figs. 5 and 6) corresponds to water forming domain structures at $R > 1$ nm (Fig. 7g).

In the case of the dried A-300/POA powder, $S_{uw} < S_{BET,A\text{-}300}$ but $S_{nano,uw} > S_{nano,N2} = 22$ m^2/g because POA forms nanocrystallites smaller than the size of silica nanoparticles (average diameter ~9 nm) and unfrozen water locates in narrow pores (voids) between silica nanoparticles and POA crystallites. Water bound in solid POA or silica/POA powders is energetically and structurally nonuniform (Fig. 7). This is due to spatial restrictions dependent on the pore (void) size distribution. There voids are between silica nanoparticles at $T > 273$ K. At $T < 273$ K ice crystallites participate in the creation of pores. There is the difference in the surface effects on water layers nearest to the surface and located in the next layers (Gun'ko et al. 2005, 2009). Therefore distant water can forms ice crystallites at higher temperatures than SBW. Bound water is characterized by the cluster size distribution (WCSD) over 0.6–10 nm in radius (Fig. 7d). Water responsible for signal 2 is nonuniform too but it does not form small clusters at $R < 1$ nm (Fig. 7g). Its nanodomains at $R = 2$–25 nm weaker interact with solid POA (Figs. 7e, f) than water responsible for signal 1.

At a low content of adsorbed water (50–100 mg/g) it tends to form small clusters (Fig. 7d). These clusters are characterized by relatively large changes in the Gibbs free energy (Figs. 7a–c). Melting of anhydrous H_3PO_4 occurs at 290 K. However, the aqueous solution of the acid can be frozen at much lower temperature because of colligative properties of the aqueous solutions (Chaplin 2011). Initial sample OX-50/H_3PO_4 (Turov et al. 2010) at $h = 5$ mg/g has only a weak ^{1}H NMR signal at $\delta_H = 4$ ppm (Fig. 8a). Its intensity decreases with lowering temperature because of freezing of water which is weakly bound to the silica surface and acid structures. Signal at $\delta_H = 0$ ppm is due to tetramethylsilane (0.2 wt.%) used as a reference compound.

In the case of dried OX-50/POA powder at $h = 45$ mg/g, the values of all the structural characteristics are much lower than those for A-300/POA at $h = 50$ mg/g (Table 2) because OX-50 has the S_{BET} value six times smaller than that of A-300. However, the difference in the S_{uw} values is smaller than that of the S_{BET} values because of contributions of POA nanocrystallites. Very large values of the structural characteristics of unfrozen water are observed for the concentrated suspension of OX-50/POA (Table 2, Fig. 9). In other words, water in this suspension is strongly clustered due to interactions with POA molecules and oligomers. To increase the amounts of water it was added to the suspension in CCl_4 stirred, shaken for 10 min and equilibrated for 2 h at 293 K.

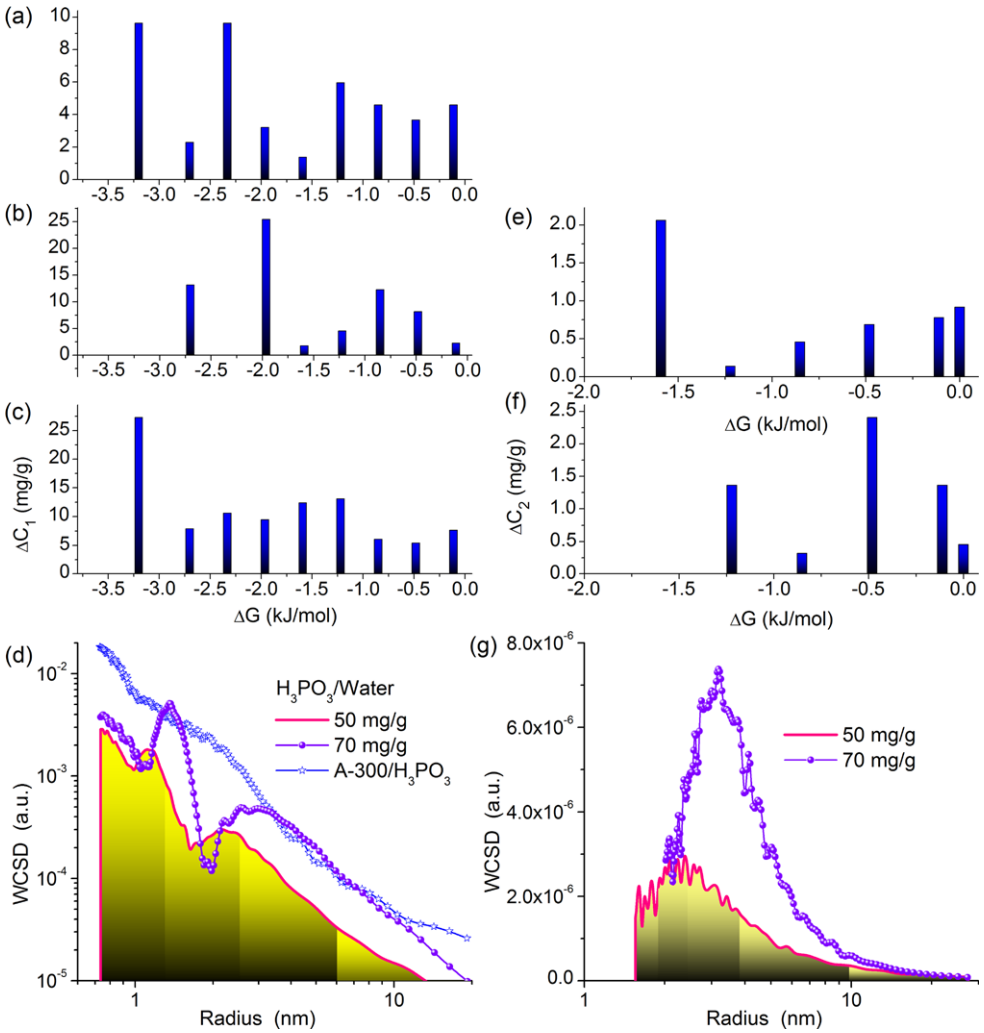

Fig. 7 Changes in the Gibbs free energy of bound water in weakly hydrated solid H_3PO_3 in CCl_4 medium at $h =$ (**a**), (**e**) 50 or (**b**), (**f**) 70 mg/g and (**c**) A-300/POA at $C_{H_2O} = 100$ mg/g and (**d**), (**g**) water cluster size distributions (WCSD) in respect to signals (**d**) 1 and (**g**) 2

The spectrum of OX-50/H_3PO_4 at $h = 25$ mg/g at 290 K (Fig. 8b) includes two signals of strongly associated water at $\delta_H = 5.5$ and 3.7 ppm and a signal of weakly associated water (WAW, characterized by $\delta_H < 2$ ppm because of a major part of the H atoms do not take part in the hydrogen bonding) at $\delta_H = 0.8$ ppm. The SAW signal at 3.7 ppm disappears at 260 K. Therefore, this water can be assigned to WBW with the size of domains larger than 10 nm in radius. Addition of water ($h = 45$ mg/g) leads to disappearance of this signal (Fig. 8c). In the case of totally unfrozen concentrated aqueous suspension of OX-50 (16 wt.%) and POA (4 wt.%) (Fig. 8d), the chemical shift increases from 4.5 ppm at 280 K to 6.5 ppm at 210 K when only a small fraction of water is unfrozen (Fig. 9b). A major amount of water is frozen at $T \leq 240$ K. Concentrating of POA in residual liquid water, whose amount decreases with decreasing temperature, results in an increase in the δ_H value.

At a low content of water ($h = 5$ and 25 mg/g), it corresponds to SBW frozen at $T < 260$ K (Fig. 9a). A small amount of WBW is observed at $h = 45$ mg/g. The δ_H value increases with decreasing temperature if $h = 25$ or 45 mg/g in contrast to that at $h = 5$ mg/g (Fig. 9b). In the last case water does not dissolve POA. The POA solubility increases with increasing h, and the δ_H value increases too. Concentrating of POA in liquid water is observed at lowering temperature because of partial freezing of bound water. In the aqueous suspension of OX-50/H_3PO_4 (Fig. 10a), the amount of bound water is larger than 3 g per gram of solids including 1 g/g of SBW. The δ_H value (related to water and PO–H groups) linearly increases to 6.7 ppm with decreasing temperature to 200 K (Fig. 10b) because of concentrating of cations formed via dissolution of POA. This temperature behavior of the δ_H value is similar to that of H_3PO_3 (Gun'ko et al. 2012a). Smaller δ_H values at higher temperatures (Fig. 10a) are due to decreased contribution of cations (formed due to dissolution of POA) with increasing temperature and thawing of frozen water.

Hydrogen peroxide as the next solute studied here has another nature than acids studied. Confined space effects may differently affect the aqueous solutions of acids and H_2O_2 that can lead to the formation of different structures of water, solutes and organic co-adsorbates located in pores. The

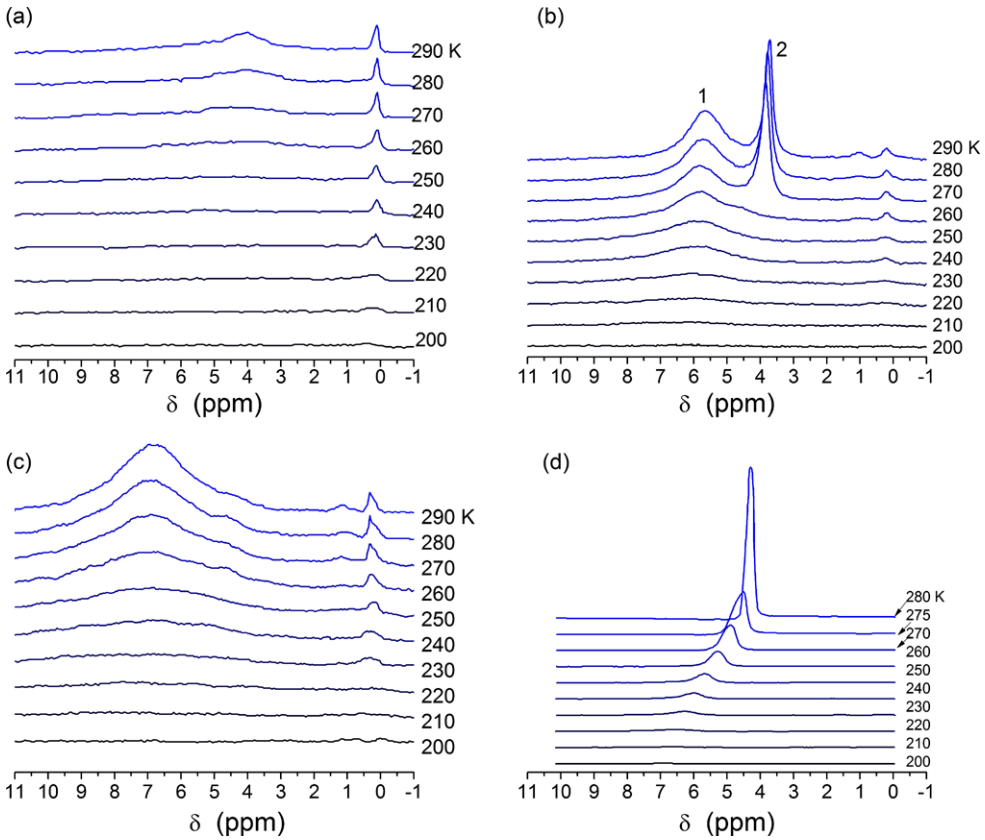

Fig. 8 ^{1}H NMR spectra recorded at different temperatures of dried OX-50/H_3PO_4 powder at $h =$ (**a**) 5, (**b**) 25 and (**c**) 45 mg/g in CCl_4 medium and (**d**) frozen aqueous suspension with OX-50 (16 wt.%) and H_3PO_4 (4 wt.%)

aqueous solution of hydrogen peroxide is characterized by two ^{1}H NMR signals at $\delta_H \approx 6$ (H_2O) and 12 (H_2O_2) ppm (Fig. 11a).

The signal width increases with increasing temperature but stronger for H_2O_2 due to enhancement of the proton exchange $H_2O \leftrightarrow H_2O_2$. A weak signal at $\delta_H \approx 2$ ppm can be assigned to methyl groups of acetone added as a standard to determine δ_H. The δ_H value of water interacting with H_2O_2 is 1–1.5 ppm greater than δ_H of bulk water (Gun'ko et al. 2009). Symbols at the peaks (Fig. 11a) show the integral intensity of the peaks. At $T < 230$ K the intensity drops down because of water and hydrogen peroxide freezing.

Complete melting of the frozen components occurs at $T_m = 250$ K. The ratio of the integral intensity of the signals is 4:1 that is close to that of their molar fractions. A decrease in the intensity at $T > T_m$ is due to changes in nuclear level population (Curie law) (Pople et al. 1959). Additionally, the H_2O_2 molecules can decompose with elimination of oxygen. This can occur in water and provide an additional channel (as paramagnetic centers) of relaxation of the nuclear magnetization. It is possible that the presence of dissolved oxygen in the H_2O_2 solution can cause a stronger manifestation of the Curie law in comparison with other similar systems (Gun'ko and Turov 2013). The H_2O_2 signal intensity (Fig. 11a) decreases with increasing temperature much stronger than that of water. This can be explained by changes in the component clusterization (due to cryoconcentration) which decreases with increasing temperature. In other words there are two states of H_2O_2 characterized by slow and fast proton exchange (in NMR time scale) and the contribution of the latter grows with increasing temperature. The models of homogeneous and clustered solutions were calculated using quantum chemical methods.

According to clustered structure of water (Chaplin 2011; Gun'ko et al. 2005, 2009), liquid water is composed of clusters and nanodomains. In the case of miscible liquids such as water and hydrogen peroxide, more clustered structure can be formed at lower temperatures (Fig. 12, cluster structure). This clustered structure can be destroyed with increasing temperature due to enhanced motion of the molecules forming a more random structure (Fig. 12, structure labeled as "solution"). The latter is characterized by broadened ^{1}H NMR spectrum theoretically calculated (Fig. 12, curves 2 and 3). In the case of the solution, the water peak shifts towards weak magnetic field (curves 2w and 3w) due to interaction of the H_2O molecules with the H_2O_2 molecules. Small clusters with anhydrous H_2O_2 have lower δ_H values (Fig. 12, curves 1, 4 and 5) than that of the solutions (curves 2 and 3). An increase in the H_2O_2 cluster size to 31 molecules and consideration for the solvation effects (curve 7) gives smaller δ_H values for H_2O_2 than that in $8H_2O_2{\cdot}20H_2O$ (curve 6) because the cluster structure in the

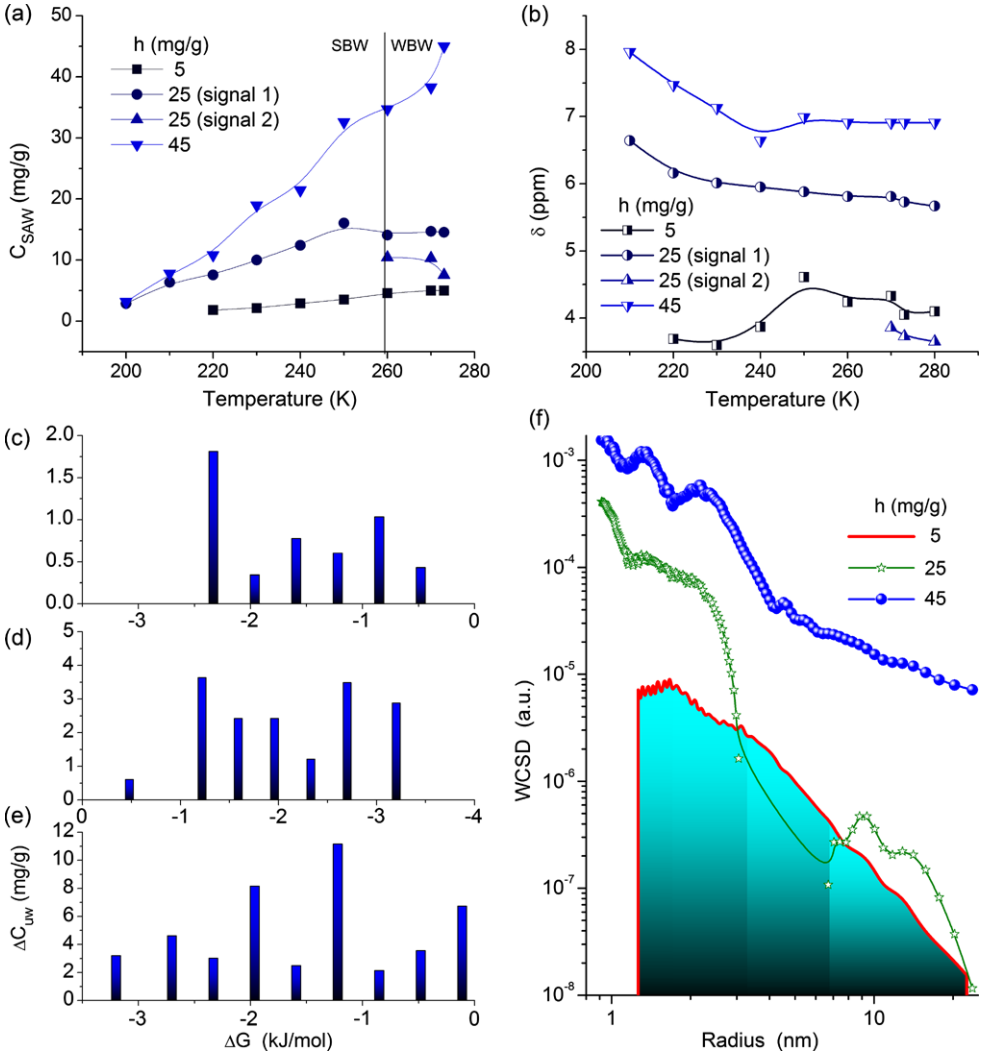

Fig. 9 Temperature dependences of (**a**) concentration of unfrozen water and (**b**) δ_H, (**c**), (**d**), (**e**) relationships between changes in the Gibbs free energy and the amounts of unfrozen water and (**f**) unfrozen water cluster size distributions for OX-50/H_3PO_4 at $h = $ (**c**) 5, (**d**) 25 and (**e**) 45 mg/g

last case differs from that without water molecules. Similar effects in the clustered (curve 2, cluster structure) and homogeneous (curve 3, solution structure) systems result in the displacement of the last spectrum towards the weak magnetic field. Interaction of the $H_2O_2 \cdot H_2O$ mixture with silica particles (in pore and at its outer surface, Fig. 13b, insert) gives a complex shape of the spectrum because of the structural nonuniformity of the system. The δ_H values are lower than that for the pure solution that is in agreement with the difference in the spectra of the solutions without and with silica (Figs. 11a–13).

At $T < 250$ K water (SAW) mixed with H_2O_2 is partially unfrozen and has a lower activity as a solvent worse dissolving H_2O_2. In other words, these liquids located in narrow pores can be only partially miscible. They tend to be more clustered in narrower pores (as shown in Fig. 12a, structure labeled as "cluster"). Greater δ_H values for water in this mixture than that for pure water is due to the hydrogen bonding with H_2O_2 molecules. With increasing temperature the solubility of H_2O_2 in SAW located in pores increases that results in enhancement of the proton exchange between water and hydrogen peroxide and its line becomes much broader. In this case, one can expect the appearance of broad but non-split signal of the H_2O–H_2O_2 mixture with down-field shift in comparison with water alone. However, this effect is absent since the separated signals of water and hydrogen peroxide are observed at $T > 250$ K (Fig. 11a). This effect can be explained by the existence of the clustered H_2O_2 structure in SAW even at 280–290 K.

In the case of interaction of the aqueous solution of H_2O_2 with nanosilica (dehydrated before mixing with the solution) placed in nonpolar (CCl_4) or weakly polar ($CDCl_3$) medium, the temperature behavior of the ^1H NMR spectra differs from that for the pure solution (Fig. 11). Several signals are in the spectra: WAW ($\delta_H \approx 1$ ppm), two signals of SAW with different amounts of dissolved H_2O_2 ($\delta_H \approx$ 5–6.5 ppm). Additionally, in the CCl_4 medium, separated signal of hydrogen peroxide is observed at $\delta_H \approx 11$ ppm. Freezing temperature of CCl_4 is 240 K; therefore, the dispersion medium freezing (Fig. 11b) results in broadening of

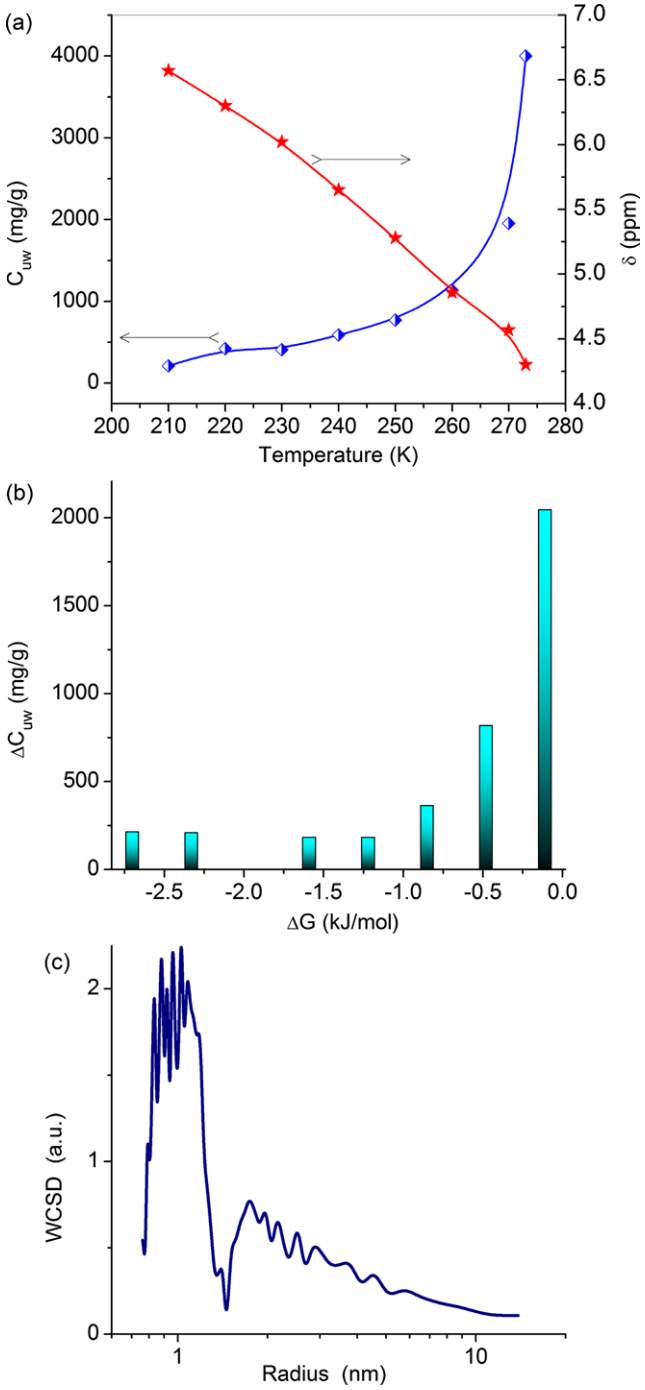

Fig. 10 Temperature dependences of (**a**) concentration of unfrozen water in concentrated suspension of OX-50 (16 wt.%) and H_3PO_4 (4 wt.%) and chemical shift δ_H, (**b**) relationship between changes in the Gibbs free energy and changes in the C_{uw} values, and (**c**) unfrozen water cluster size distribution

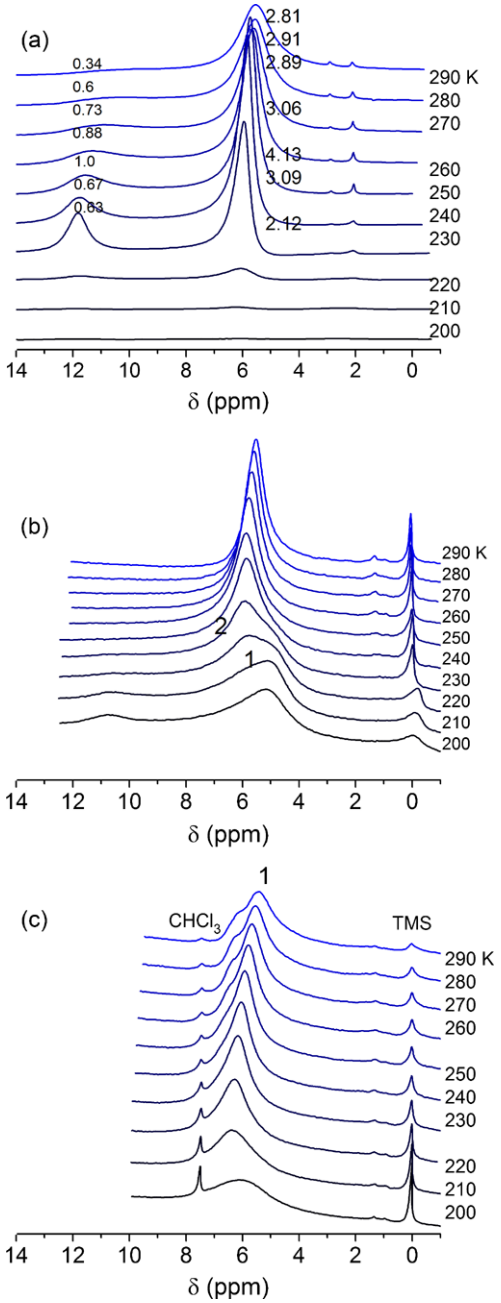

Fig. 11 ^{1}H NMR spectra of aqueous 30 % solution of H_2O_2 (**a**) bulk and adsorbed (10 wt.%) onto A-400 being in (**b**) CCl_4 and (**c**) $CDCl_3$ media

TMS signal at $\delta_H = 0$ ppm. Near freezing temperature of CCl_4 transition of SAW from state 1 at $\delta_H \approx 5$ ppm into state 2 at $\delta_H \approx 6$ ppm is observed. Both signals are observed at 210–240 K. The H_2O_2 signal decreases with temperature and it disappears at $T > 240$ K (Fig. 11b).

In weakly polar $CDCl_3$ medium (Fig. 11c), the signal of H_2O_2 is not observed, however, the baseline increases towards the weak field (i.e. the signal becomes too broad). The δ_H value of SAW increases. Splitting of the SAW peak into 1 and 2 states occurs at $T > 250$ K. Signal 2 shifts towards strong magnetic field with increasing temperature because of decreasing clusterization of the solution. This effect for signal 1 is much smaller. Silica A-400 as a nanostructured material affects the clusterization of the solution located in

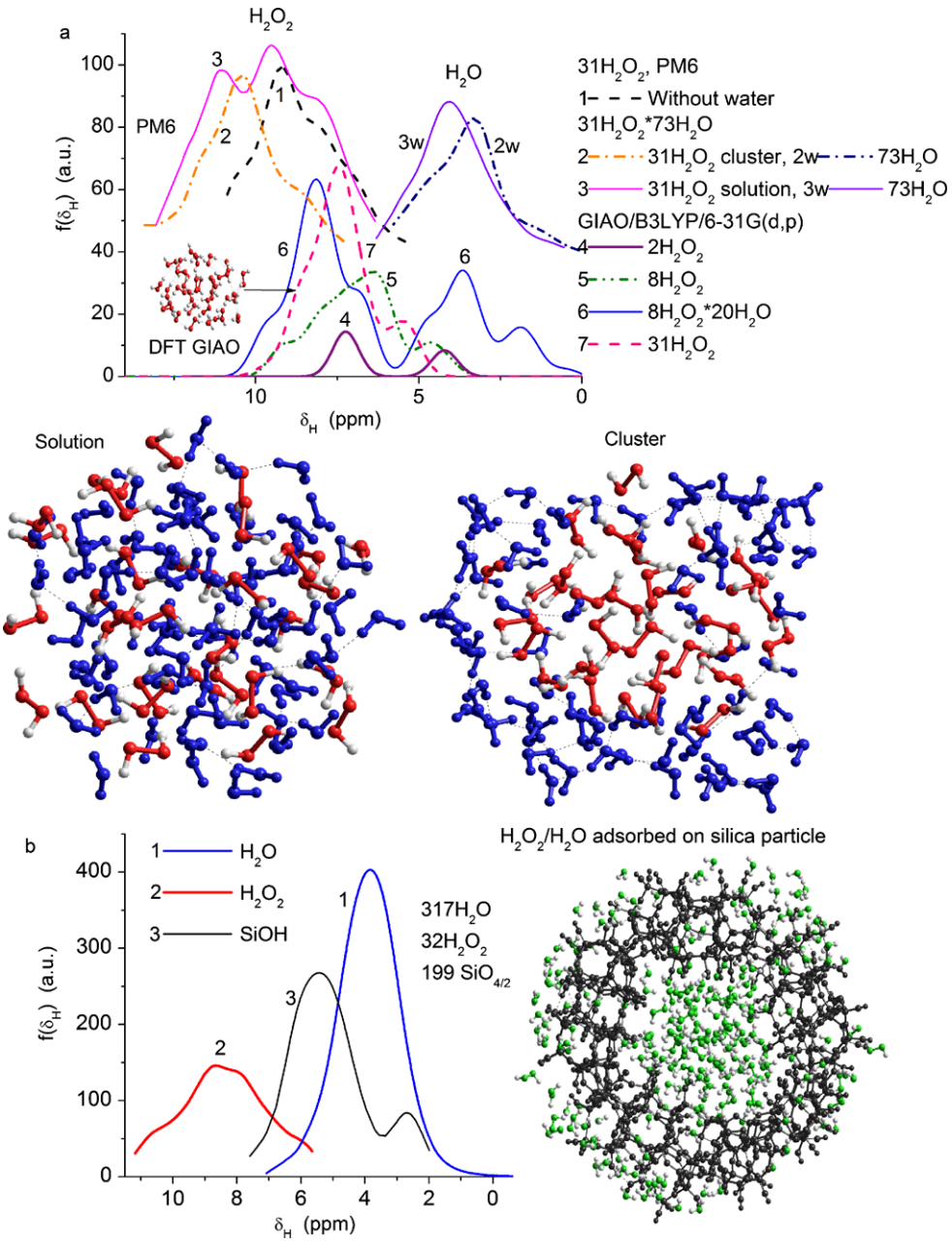

Fig. 12 ^{1}H NMR spectra of clusters calculated using PM6 method and the correlation functions for water and hydrogen peroxide based on the GIAO/DFT and PM6 calculations of the same systems ((**a**), *curves* 1–3, and (**b**), GIAO/B3LYP/6-31G(d,p) ((**a**), *curves* 4–6) and GIAO/IEFPCM/B3LYP/6-31G(d,p) ((**a**), *curve* 7) with (**a**) hydrogen peroxide alone or with water molecules; two types of the mixtures were shown with pure solution (*curve* 3) and clustered (*curve* 2) structures; and (**b**) $317H_2O{\cdot}32H_2O_2$ adsorbed onto silica particles (199 tetrahedrons)

narrow nano- and mesopores (voids between silica nanoparticles, Fig. 2). This process depends also on cryoconcentration, i.e. relative concentration of H_2O_2 in certain structures increases due to partial freezing of water.

The ^{1}H NMR spectra of the H_2O/H_2O_2 mixture adsorbed onto nanosilica being in different mixtures of nonpolar (CCl_4) or weakly polar ($CDCl_3$) solvent with addition of polar solvents (CD_3CN, $(CD_3)_2SO$) (Fig. 13) demonstrate complex temperature behavior.

Besides signals of water, H_2O_2 and TMS, signals of methyl groups of CH_3CN (as admixture in CD_3CN) at $\delta_H = 2.2$ ppm and $(CH_3)_2SO$ (admixture in $(CD_3)_2SO$) at $\delta_H = 2.5$ ppm are observed. In frozen CCl_4 medium ($T <$ 240 K) signals of SAW and H_2O_2 are observed separately (Fig. 13a). The SAW signal demonstrates up-field shift with increasing temperature and a minimal value $\delta_H = 3.5$ ppm is observed at 230 K and then has down-field shift. At 240 K two signals of H_2O_2 in the adsorbed solution are observed at $\delta_H = 10$ and 8.5 ppm. However, at higher temperatures only one weak signal is observed and its δ_H value decreases with temperature. Since the δ_H value of this signal is lower than that of pure H_2O_2 one can assume that the H_2O_2 molecules form clusters with water and acetonitrile molecules. The proton exchange reactions of H_2O_2 with H_2O results in signal broadening and intensity decreasing of the peak depending on the type of added solvent. After melting of CCl_4

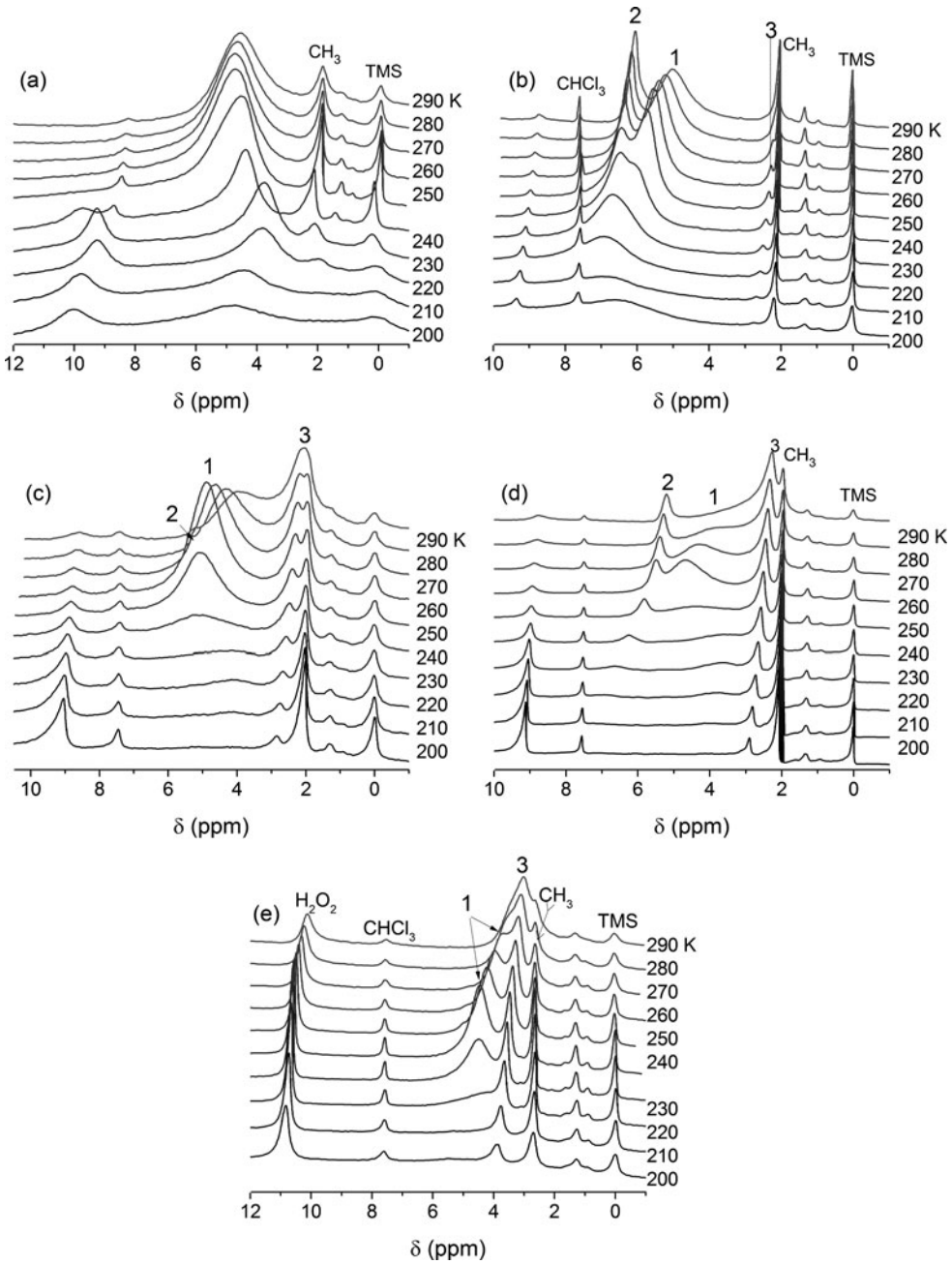

Fig. 13 ^{1}H NMR spectra of aqueous 30 % solution of H_2O_2 adsorbed (10 wt.%) onto A-400 being in (**a**) $CCl_4 + 8$ % CD_3CN, (**b**) $CDCl_3 + 8$ % CD_3CN, (**c**) $CDCl_3 + 15$ % CD_3CN, (**d**) $CDCl_3 + 22$ % CD_3CN, (**e**) $CDCl_3 + 8$ % DMSO media

($T > 240$ K) a major portion of H_2O_2 dissolves in the SAW nanodomains (that result in increasing δ_H value of SAW) or forms the adsorption complexes with surface silanols groups (Fig. 13a). In the last case their signal can be absent in the spectra due to the proton exchange SiOH ↔ HOH causing significant shortening of the relaxation time.

In the $CDCl_3$ with addition of CD_3CN (Fig. 13b), a weak signal of H_2O_2 is observed at $\delta_H \approx 9$ ppm. It can be due to the formation of clusters with the participation of H_2O_2, H_2O and $CDCl_3$ or CD_3CN molecules (as well as in the system shown in Fig. 13a). SAW is observed as one ($T <$ 240 K) or two signals (signals 1 and 2) with up-field shift with increasing temperature. Signal 1 has a greater shift than signal 2. The maximal δ_H value for SAW is 7 ppm at 220 K. At lower temperatures, the signal intensity and its δ_H value decrease due to partial freezing of water and H_2O_2. Weak signal of water (signal 3) is also observed at $\delta_H = 2.2$–2.4 ppm (to the left from the signal of methyl groups of acetonitrile). This δ_H value is intermediate between the values of WAW (1–1.5 ppm) and water associated (ASW) with acetonitrile molecules (3 ppm). This signal intensity increases with increasing concentration of acetonitrile in the mixture with CD_3Cl (Figs. 13b–d). It is possible that it can be caused by clusters with CD_3Cl–CD_3CN–H_2O

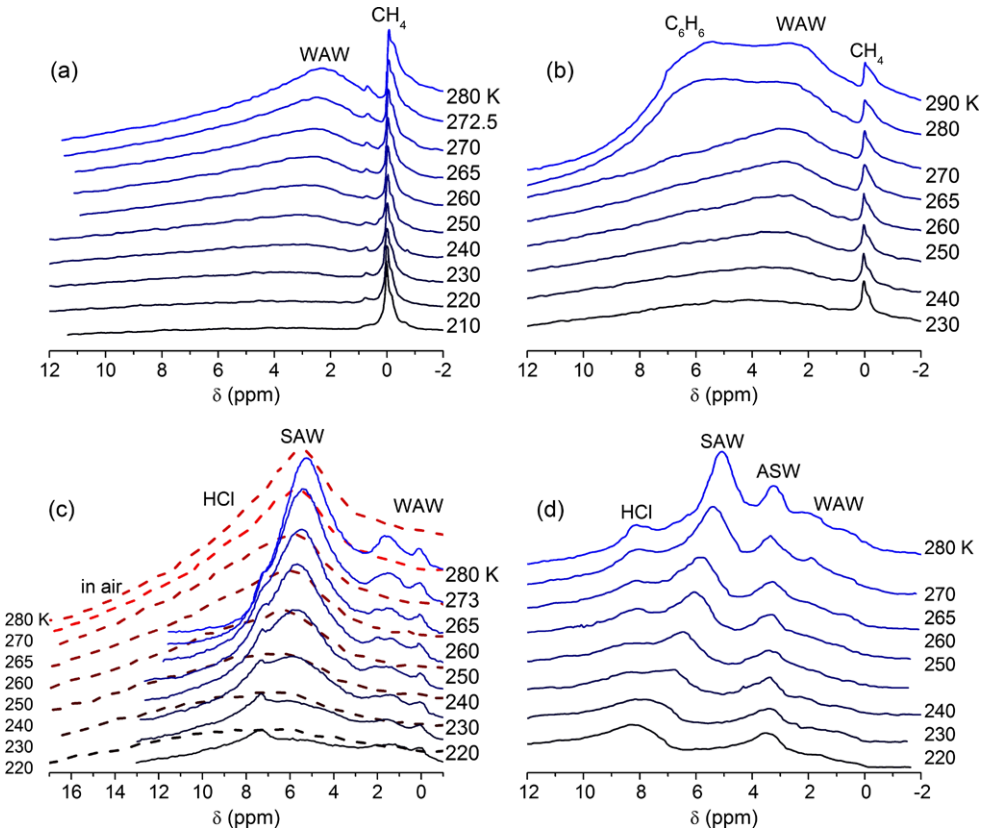

Fig. 14 ^{1}H NMR spectra of water ((**a**), (**b**) hydration $h = 0.1$, (**c**) 0.3 and (**d**) 0.5 g/g) co-adsorbed with (**a**) methane (from reservoir at pressure of 1.1 bar), (**b**) +1 g/g benzene and methane; (**c**) 0.1 g/g HCl in air (*dashed lines*) or $CDCl_3$ (*solid lines*) dispersion medium; and (**d**) 0.2 HCl (in $CDCl_3$ + DMSO) bound to MLGO

bound to the A-400 surface in narrow voids (Fig. 2). The H_2O_2 signal intensity at $\delta_H \approx 9$ ppm increases with increasing CD_3CN concentration (Figs. 13b–d). The minimal δ_H value of SAW decreases to 4 ppm. Signals 1 and 2 are observed separately only at $T > 270$ K. Signal 3 is the most intensive at 22 % CD_3CN in the mixture with CD_3Cl. It intensity increases with increasing temperature but intensity of signal 1 decreases. In the case of a $CDCl_3$ mixture with DMSO (Fig. 13e), the δ_H value of hydrogen peroxide increases to 11 ppm. Significant changes in the intensity of signals 3 and 1 (similar to that at 22 % CD_3CN) are observed at 5 % DMSO added to CD_3Cl.

MLGO has the texture which significantly differs from that of nanosilicas. MLGO is composed of large (200–800 nm) carbon sheets forming relatively thin stacks with 5–6 carbon sheets. Carbon sheets include a great amount of O-containing functionalities (∼10 at.%) of different structures. Water can be bound to the O-containing functionalities in the form of clusters (Gun'ko et al. 2012b).

The spectra of the HCl solution adsorbed to MLGO depend on co-adsorbate content and the type of dispersion medium (Fig. 14). An increase in the water and HCl amounts and replace of air by chloroform alone or in mixture with DMSO leads to appearance of signal at $\delta_H = 9$ ppm characteristic for concentrated HCl solution (Turov et al. 2011). The down-field shift is observed with decreasing temperature due to two effects: (i) concentrating HCl solution in SAW, and (ii) stronger interactions of close located layers of unfrozen liquids to the surface with the O-functionalities.

In the case of the $CDCl_3$ medium, the spectra change (Fig. 14). The main signal demonstrates a certain up-field shift (by 0.5 ppm). Signal of concentrated HCl solution ($\delta_H \approx 9$ ppm) is not observed but signal of weakly associated water (WAW) appears at $\delta_H \approx 1.5$ ppm. An increase in the dispersion medium polarity by addition of 10 % of DMSO results in the spectra (Fig. 14d) including 4–5 signals.

The temperature behavior of these signals differs. For instance, signal of water associated with DMSO molecules (ASW) at $\delta_H \approx 3.5$ ppm does not change the position in contrast to signal of SAW at $\delta_H \approx 5$ ppm at 280 K (with small content of HCl dissolved in bound water) and 7 ppm at 240 K. The latter is due to changes in the content of HCl in SAW at decreasing temperature because of acid concentrating effect. Therefore, only one signal ($\delta_H \approx 8.5$ ppm) of HCl/SAW is observed at 220 K. In contrast to SAW, WAW cannot dissolve HCl. Therefore, the signal position of WAW at $\delta_H \approx 1.5$ ppm does not change at decreasing temperature.

4 Conclusions

Hydrochloric acid being in contact with silica nanoparticles placed in nonpolar (CCl_4) or weakly polar ($CDCl_3$) media

forms clusters of two types (with different content of water and HCl) in interparticle voids of the silica powder. This suggests that the aqueous solution of HCl is divided into certain components at the silica surface. This dividing is stronger in the case mechanochemically activated silica at higher bulk density because of enhanced effects of confined space in narrower pores. Temperature affected clusterization of the HCl solution is also observed at the surface of MLGO.

Concentrated solutions or weakly hydrated solid phosphorus oxyacids (POA) or dried nanosilica/POA powders being in the CCl_4 medium are characterized by different temperature dependences of the chemical shift of the proton resonance (δ_H) because of partial dissociation of PO–H bonds strongly depending on water amounts and temperature. NMR cryoporometry results show that both small water clusters and nanodomains are present at the interfaces of hydrated solid POA and silica/POA powders.

Interactions of 30 % aqueous solution of H_2O_2 with nanosilica in the nonpolar CCl_4 or CD_3Cl media with addition of polar co-solvents CD_3CN or $(CD_3)_2SO$ into the nonpolar medium are accompanied by the formation of two types of structures with strongly associated water ($\delta_H = 4$–6 ppm) including different amounts of H_2O_2. The H_2O/H_2O_2 structures bound to silica in weakly polar CD_3Cl with addition of CD_3CN or DMSO form three types of clusters with: (i) concentrated H_2O_2 at $\delta_H = 9$–11 ppm; (ii) concentrated water and dissolved polar co-solvents; and (iii) organic co-solvents containing certain amounts of water and H_2O_2.

Thus, clusterization of higher and lower concentrated acid solutions (in SAW) and nearly pure water (with WAW) occurs at the interfaces of different adsorbents. This clusterization depends strongly on the type of dispersion medium, especially its polarity. Obtained results show some ways to control the interfacial structures in complex systems.

Acknowledgements The authors are grateful European Community, Seventh Framework Programme (FP7/2007-2013), Marie Curie International Research Staff Exchange Scheme (grant No. 230790).

References

Brennan, J.K., Bandosz, T.J., Thomson, K.T., Gubbins, K.E.: Water in porous carbons. Colloids Surf. A, Physicochem. Eng. Asp. **187–188**, 539–568 (2001)

Chaplin, M.: Water structure and science (2011). http://www.lsbu.ac.uk/water/

Derjaguin, B.V., Churaev, N.V., Muller, V.M.: Surface Forces. Consultants Bureau, New York (1987)

Derjaguin, B.V., Ovcharenko, F.D., Churaev, N.V. (eds.): Water in Disperse Systems. Khimiya, Moscow (1989)

Drago, R.S.: Physical Methods in Chemistry. Saunders, Philadelphia (1977)

Emsley, J.W., Feenej, J., Sutcliffe, L.H.: High Resolution Nuclear Magnetic Resonance Spectroscopy. Pergamon, Oxford (1965)

Frisch, M.J., Trucks, G.W., Schlegel, H.B., Scuseria, G.E., Robb, M.A., Cheeseman, J.R., Montgomery, J.A., Vreven, T. Jr., Kudin, K.N., Burant, J.C., Millam, J.M., Iyengar, S.S., Tomasi, J., Barone, V., Mennucci, B., Cossi, M., Scalmani, G., Rega, N., Petersson, G.A., Nakatsuji, H., Hada, M., Ehara, M., Toyota, K., Fukuda, R., Hasegawa, J., Ishida, M., Nakajima, T., Honda, Y., Kitao, O., Nakai, H., Klene, M., Li, X., Knox, J.E., Hratchian, H.P., Cross, J.B., Adamo, C., Jaramillo, J., Gomperts, R., Stratmann, R.E., Yazyev, O., Austin, A.J., Cammi, R., Pomelli, C., Ochterski, J.W., Ayala, P.Y., Morokuma, K., Voth, G.A., Salvador, P., Dannenberg, J.J., Zakrzewski, V.G., Dapprich, S., Daniels, A.D., Strain, M.C., Farkas, O., Malick, D.K., Rabuck, A.D., Raghavachari, K., Foresman, J.B., Ortiz, J.V., Cui, Q., Baboul, A.G., Clifford, S., Cioslowski, J., Stefanov, B.B., Liu, G., Liashenko, A., Piskorz, P., Komaromi, I., Martin, R.L., Fox, D.J., Keith, T., Al-Laham, M.A., Peng, C.Y., Nanayakkara, A., Challacombe, M., Gill, P.M.W., Johnson, B., Chen, W., Wong, M.W., Gonzalez, C., Pople, J.A.: Gaussian 03 Revision E.01. Gaussian, Inc., Wallingford, CT (2004)

Glushko, V.P. (ed.): Handbook of Thermodynamic Properties of Individual Substances. Nauka, Moscow (1978) (in Russian)

Gregg, S.J., Sing, K.S.W.: Adsorption, Surface Area and Porosity. Academic Press, London (1982)

Gun'ko, V.M., Mikhalovsky, S.V.: Evaluation of slitlike porosity of carbon adsorbents. Carbon **42**, 843–849 (2004)

Gun'ko, V.M., Turov, V.V.: Nuclear Magnetic Resonance Studies of Interfacial Phenomena. Taylor & Francis, San Diego (2013, in press)

Gun'ko, V.M., Turov, V.V., Bogatyrev, V.M., Zarko, V.I., Leboda, R., Goncharuk, E.V., Novza, A.A., Turov, A.V., Chuiko, A.A.: Unusual properties of water at hydrophilic/hydrophobic interfaces. Adv. Colloid Interface Sci. **118**, 125–172 (2005)

Gun'ko, V.M., Turov, V.V., Gorbik, P.P.: Water at the Interfaces, Naukova Dumka, Kiev (2009) (in Russian)

Gun'ko, V.M., Morozova, L.P., Turova, A.A., Turov, A.V., Gaishun, V.E., Bogatyrev, V.M., Turov, V.V.: Hydrated phosphorus oxyacids alone and adsorbed on nanosilica. J. Colloid Interface Sci. **368**, 263–272 (2012a)

Gun'ko, V.M., Turov, V.V., Whitby, R.L.D., Prykhod'ko, G.P., Turov, A.V., Mikhalovsky, S.V.: Interactions of single and multi-layer graphene oxides with water, methane, organic solvents and HCl studied by ^{1}H NMR method. Carbon (2012b, submitted for publication)

Hess, W.T.: Hydrogen peroxide. In: Kirk-Othmer Encyclopedia of Chemical Technology, 4th edn., vol. 13, pp. 961–995. Wiley, New York (1995)

Israelachvili, J.N., Wennerstrom, H.: Hydration or steric forces between amphiphilic surfaces? Langmuir **6**, 873–876 (1990)

Jieli, M., Aida, M.: Classification of OH bonds and infrared spectra of the topology-distinct protonated water clusters $H_3O^+(H_2O)_{n-1}$ ($n \leq 7$). J. Phys. Chem. A **113**, 1586–1594 (2009)

Jones, C.W.: Applications of Hydrogen Peroxide and Derivatives. Royal Chem. Soc., Cambridge (1999)

Leninsky, M.I., Mazanko, A.F., Novikov, I.N.: Hydrogen Chloride and Hydrochloric Acid. Khimiya, Moscow (1985)

March, J.: Advanced Organic Chemistry, 4th edn. Wiley, New York (1992)

Mitchell, J., Webber, J.B.W., Strange, J.H.: Nuclear magnetic resonance cryoporometry. Phys. Rep. **461**, 1–36 (2008)

Murakhtina, T., Heuft, J., Meijer, E.J., Sebastiani, D.: First principles and experimental ^{1}H NMR signatures of solvated ions: the case of HCl(aq). Chem. Phys. Chem. **7**, 2578–2584 (2006)

Nekrasov, B.V.: Fundamentals of General Chemistry. Khimya, Moscow (1973)

Petrov, O.V., Furó, I.: NMR cryoporometry: principles, applications and potential. Prog. Nucl. Magn. Reson. Spectrosc. **54**, 97–122 (2009)

Pople, J.A., Schneider, W.G., Bernstein, H.J.: High-Resolution Nuclear Magnetic Resonance. McGraw-Hill, New York (1959)

Schuster, M., Kreuer, K.-D., Steininger, H., Maier, J.: Proton conductivity and diffusion study of molten phosphonic acid H_3PO_3. Solid State Ion. **179**, 523–528 (2008)

Stephenson, N.A., Bell, A.T.: Quantitative analysis of hydrogen peroxide by ^{1}H NMR spectroscopy. Anal. Bioanal. Chem. **381**, 1289–1293 (2005)

Stewart, J.J.P.: MOPAC2012. Stewart Computational Chemistry, Colorado Springs, CO, USA. http://openmopac.net/MOPAC2012.html (2012)

Strange, J.H., Rahman, M., Smith, E.G.: Characterization of porous solids by NMR. Phys. Rev. Lett. **71**, 3589–3591 (1993)

Tolstoy, P.M., Smirnov, S.N., Shenderovich, I.G., Golubev, N.S., Denisov, G.S., Limbacha, H.-H.: NMR studies of solid state—solvent and H/D isotope effects on hydrogen bond geometries of 1:1 complexes of collidine with carboxylic acids. J. Mol. Struct. **700**, 19–27 (2004)

Turov, V.V., Gun'ko, V.M.: Clustered Water and Ways of Its Applications. Naukova Dumka, Kiev (2011)

Turov, V.V., Gun'ko, V.M., Zarko, V.I., Bogatyr'ov, V.M., Dudnik, V.V., Chuiko, A.A.: Water adsorption at pyrogenic silica surfaces modified by phosphorus compounds. Langmuir **12**, 3503–3510 (1996)

Turov, V.V., Gun'ko, V.M., Gaishun, V.E., Kosenok, Y.A., Golovan, A.P.: Application of NMR spectroscopy to determine the thermodynamic characteristics of water bound to OX-50 nanosilica. J. Appl. Spectrosc. **77**, 588–594 (2010)

Turov, V.V., Gun'ko, V.M., Turova, A.A., Morozova, L.P., Voronin, E.F.: Interfacial behavior of concentrated HCl solution and water clustered at a surface of nanosilica in weakly polar solvents media. Colloids Surf. A, Physicochem. Eng. Asp. **390**, 48–55 (2011)

Zhang, S.: Direct detection of hydrogen peroxide via ^{1}H CEST-MRI. Proc. Int. Soc. Magn. Reson. Med. **15**, 3461 (2007)